AIAA JOURNAL
Vol. 36, No. 4, April 1998

Design Sensitivity Analysis of Hyperelastic Structures Using a Meshless Method

Iulian Grindeanu*
University of Iowa, Iowa City, Iowa 52242
Kuang-Hua Chang†
University of Oklahoma, Norman, Oklahoma 73019-4076
and
Kyung K. Choi‡ and Jiun-Shyan Chen§
University of Iowa, Iowa City, Iowa 52242

A continuum-based design sensitivity analysis method for hyperelastic structures is presented. Analysis is performed using a meshless method, called the reproducing kernel particle method. Yeoh's energy density function is used to describe the hyperelastic structural behavior. The meshless method eliminates mesh distortion or entanglement encountered in using finite element analysis for large deformation structural analysis and structural shape design optimization. Both the adjoint variable and direct differentiation methods are developed for material and shape design variables. An infinitely long rubber tube, a two-dimensional rubber band, and an engine mount are examples used to demonstrate the feasibility and accuracy of the method.

Nomenclature

a	= dilation parameter
$a({}^{t+\Delta t}\mathbf{z}, {}_0\bar{\mathbf{z}})$	= energy form (linear in virtual displacements)
$a^*({}^t_0\mathbf{z}; {}_0\mathbf{z}, {}_0\bar{\mathbf{z}})$	= energy bilinear form
$C(x; x-s)$	= correction function
${}_0D_{ijkl}$	= incremental stress-strain tensor components
${}_0e_{ij}$	= linear part of strain increments
${}^t_0F_{ij}$	= deformation tensor components, $\partial {}^tx_i/\partial X_j = \delta_{ij} + \partial {}^tz_i/\partial X_j$
${}^t_0\boldsymbol{G}$	= right Cauchy–Green deformation tensor, $({}^t_0\boldsymbol{F})^T {}^t_0\boldsymbol{F}$
$\mathcal{L}({}_0\bar{\mathbf{z}})$	= load form (virtual external work), $\equiv {}^{t+\Delta t}R$
$\boldsymbol{M}(x)$	= moment matrix at x
$m_n(x)$	= moment of order n at x
${}^t_0S_{ij}$	= second Piola–Kirchhoff stress components
${}_0S_{ij}$	= increments for stress components, ${}^{t+\Delta t}_0S_{ij} - {}^t_0S_{ij}$
${}^t_0W$	= strain energy density function
$\boldsymbol{X}$	= position of a material particle at initial configuration
${}^t\boldsymbol{x}$	= position of a material particle at time t
${}^t_0\mathbf{z}$	= displacement vector referred to the original configuration, ${}^t\boldsymbol{x} - \boldsymbol{X}$
${}_0\mathbf{z}$	= increment in displacement vector, ${}^{t+\Delta t}_0\mathbf{z} - {}^t_0\mathbf{z}$
${}_0\bar{\mathbf{z}}$	= virtual displacement vector
${}^t\Gamma$	= boundary of domain at time t
δ	= Kronecker symbol
${}^t_0\varepsilon_{ij}$	= Green–Lagrangian strain components, $\frac{1}{2}({}^t_0G_{ij} - \delta_{ij}) = \frac{1}{2}({}^tz_{i,j} + {}^t_0z_{j,i} + {}^t_0z_{k,i}\,{}^t_0z_{k,j})$
${}_0\varepsilon_{ij}$	= increments for strain components, ${}^{t+\Delta t}_0\varepsilon_{ij} - {}^t_0\varepsilon_{ij}$
${}_0\eta_{ij}$	= nonlinear part of strain increments
Φ_a	= kernel function
$\bar{\Phi}_a(x; x-s)$	= modified kernel function
$\Psi_I(x)$	= interpolation function of particle X_I
ψ	= generic performance measure
${}^t\Omega$	= physical domain at time t
$(\,)'$	= first-order variation with respect to a material property design variable u
$\dot{(\,)}$	= total derivative with respect to a shape design variable

Received March 17, 1997; revision received Nov. 27, 1997; accepted for publication Jan. 2, 1998.

*Research Assistant, Center for Computer-Aided Design and Department of Mechanical Engineering, College of Engineering. E-mail: igrindea@ccad.uiowa.edu.

†Assistant Professor, School of Aerospace and Mechanical Engineering. E-mail: khchang@ou.edu.

‡Professor and Director, Center for Computer-Aided Design and Department of Mechanical Engineering, College of Engineering. E-mail: kkchoi@ccad.uiowa.edu.

§Assistant Professor, Center for Computer-Aided Design and Department of Mechanical Engineering, College of Engineering. E-mail: jschen@icaen.uiowa.edu.

I. Introduction

ONE of several challenges in structural shape optimization involves mesh distortion or entanglement during design iterations due to shape changes, when the finite element method (FEM) is used for structural analysis. Consequently, shape optimization iterations often fail or converge to an unacceptable solution. Similar problems exist in using finite element analysis (FEA) for structural analysis of large deformation nonlinear problems, such as hyperelastic structures and metal forming, in which the finite element mesh is distorted or entangled due to excessive deformation.

In recent years, a number of meshless methods not requiring explicit mesh have been developed. Smooth particle hydrodynamics (SPH)[1] was the first meshless method developed for infinite domain astronomy problems; however, the solution accuracy was unsatisfactory when SPH was applied to structural problems. The diffuse element method (DEM)[2] was introduced based on moving least-squares approximation. The element-free Galerkin[3,4] method improved the solution accuracy of DEM through a better numerical integration method, inclusion of the derivatives of interpolants that were omitted in DEM, and an accurate treatment of essential boundary conditions. The reproducing kernel particle method (RKPM)[5–8] was proposed to improve the accuracy of SPH for finite domain problems. In RKPM, the kernel function was modified by introducing a correction function to meet the reproducing conditions. The resulting modified kernel function exactly reproduces polynomials to a specific order and thereby fulfills the completeness requirement.[5] The shape functions developed from RKPM were later proved to be equivalent to moving least-squares kernel interpolants if polynomial basis functions were used.[9] The RKPM was extended to highly nonlinear hyperelasticity[7] and elastoplasticity[8] problems by introducing a material kernel function to handle extreme material distortion without readjustment of dilation parameters. A direct transformation method[7,8] was also introduced to exactly impose essential boundary conditions. This approach successfully resolves mesh distortion

problems, and very accurate solutions can be obtained with relatively fewer degrees of freedom compared with FEM.[7,8]

Considerable work has been devoted recently to nonlinear design sensitivity analysis (DSA), for both sizing[10–16] and shape[15–20] design applications. Both the material derivative method[18] and the control volume method[19,20] were used for shape DSA. Choi and Duan[17] developed a DSA method for hyperelastic structures using ABAQUS.[21] A mesh distortion problem occurred in the FEA of a two-dimensional engine mount example using ABAQUS, when large loads were applied.

Our objective here is to develop a DSA method for hyperelastic structures using RKPM. In this work, both the material and shape design variables are considered for DSA. For continuum-based DSA, the tangent stiffness operator at the final equilibrium configuration is used to derive the adjoint and sensitivity equations. Consequently, computation of the sensitivity coefficient is efficient because no iterations are needed to achieve a convergent solution. Also, the tangent stiffness matrix at the final equilibrium configuration was decomposed during the structural analysis process; only forward and backward substitutions are needed for DSA.

Organization of the remainder of the paper is as follows: Sec. II presents a variational equation of hyperelastic structure and its linearized incremental form. Section III is an overview of the RKPM and its discretized form. Sections IV and V describe the proposed material and shape DSA methods using RKPM. Section VI describes a numerical method for DSA using RKPM. An infinitely long rubber tube, a two-dimensional rubber band, and an engine mount are presented as examples in Sec. VII to demonstrate the proposed method. Section VIII presents a summary and future research directions.

II. Variational Equations of Nonlinear Hyperelastic Structures

Using the principle of virtual work, we can write the equilibrium equation of a hyperelastic structure at the configuration of time $t+\Delta t$, with domain ${}^{t+\Delta t}\Omega$ and boundary ${}^{t+\Delta t}\Gamma$ as[22]

$$\int_{{}^{t+\Delta t}\Omega} {}^{t+\Delta t}\bar{W}\ {}^{t+\Delta t}\mathrm{d}\Omega = {}^{t+\Delta t}R \tag{1}$$

where ${}^{t+\Delta t}R$ is the virtual work done on the structure by the externally applied load through a kinematically admissible virtual displacement. The overbar represents the first-order variation of the quantity. Using Yeoh's strain energy density[23] definition expressed by Penn's reduced invariants (Ref. 24), ${}^{t+\Delta t}W$ can be written as

$$\begin{aligned} {}^{t+\Delta t}W &= A_{10}\left({}^{t+\Delta t}_{0}\hat{I}_1 - 3\right) + A_{20}\left({}^{t+\Delta t}_{0}\hat{I}_1 - 3\right)^2 \\ &\quad + A_{30}\left({}^{t+\Delta t}_{0}\hat{I}_1 - 3\right)^3 + (k/2)\left({}^{t+\Delta t}_{0}J - 1\right)^2 \end{aligned} \tag{2}$$

where A_{10}, A_{20}, A_{30}, and k are material properties. In Eq. (2),

$$\begin{gathered} {}^{t+\Delta t}_{0}\hat{I}_1 = {}^{t+\Delta t}_{0}I_1\left({}^{t+\Delta t}_{0}I_3\right)^{-\frac{1}{3}}, \qquad {}^{t+\Delta t}_{0}I_1 = \mathrm{tr}\left({}^{t+\Delta t}_{0}\boldsymbol{G}\right) \\ {}^{t+\Delta t}_{0}I_3 = \det\left({}^{t+\Delta t}_{0}\boldsymbol{G}\right) \end{gathered} \tag{3a}$$

and

$${}^{t+\Delta t}_{0}J = \left({}^{t+\Delta t}_{0}I_3\right)^{\frac{1}{2}} = \det\left({}^{t+\Delta t}_{0}\boldsymbol{F}\right) \tag{3b}$$

where ${}^{t+\Delta t}_{0}\boldsymbol{F}$ is the deformation gradient tensor and ${}^{t+\Delta t}_{0}\boldsymbol{G} = ({}^{t+\Delta t}_{0}\boldsymbol{F})^T({}^{t+\Delta t}_{0}\boldsymbol{F})$ is the right Cauchy–Green deformation tensor.

For the total Lagrangian formulation, the initial configuration at $t=0$ is selected as the reference configuration, and the second Piola–Kirchhoff stress tensor ${}^{t+\Delta t}_{0}S_{ij}$ and the Green–Lagrangian strain tensor ${}^{t+\Delta t}_{0}\varepsilon_{ij}$ are employed. We can write the equilibrium Eq. (1) as[10]

$$\begin{aligned} a\left({}^{t+\Delta t}_{0}z, {}_0\bar{z}\right) &\equiv \int_{0_\Omega} {}^{t+\Delta t}\bar{W}\ {}^{0}\mathrm{d}\Omega = \int_{0_\Omega} {}^{t+\Delta t}_{0}S_{ij}\ {}^{t+\Delta t}_{0}\bar{\varepsilon}_{ij}\ {}^{0}\mathrm{d}\Omega \\ &= \int_{0_\Omega} {}^{t+\Delta t}_{0}f_i\ {}_0\bar{z}_i\ {}^{0}\mathrm{d}\Omega + \int_{0_\Gamma} {}^{t+\Delta t}_{0}T_i\ {}_0\bar{z}_i\ {}^{0}\mathrm{d}\Gamma \equiv \ell({}_0\bar{z}) \\ &\qquad \text{for all} \quad {}_0\bar{z} \in {}_0Z \end{aligned} \tag{4}$$

where ${}^{t+\Delta t}_{0}z$ is structural displacement at time $t+\Delta t$ referred to the configuration at time 0, ${}^{t+\Delta t}_{0}f_i$ and ${}^{t+\Delta t}_{0}T_i$ are structural body force and traction force, ${}^{0}\Omega$ and ${}^{0}\Gamma$ are the structural domain and boundary, and ${}_0Z$ is the space of kinematically admissible virtual displacements. Stress components for assumed hyperelastic material are computed using[25,26]

$$\begin{aligned} {}^{t+\Delta t}_{0}S_{ij} &= {}^{t+\Delta t}_{0}W_{,\varepsilon_{ij}} = \frac{\partial\, {}^{t+\Delta t}_{0}W}{\partial\, {}^{t+\Delta t}_{0}\varepsilon_{ij}} \\ &= 2\left\{\left[A_{10} + 2A_{20}\left({}^{t+\Delta t}_{0}\hat{I}_1 - 3\right) + 3A_{30}\left({}^{t+\Delta t}_{0}\hat{I}_1 - 3\right)^2\right]\right. \\ &\quad \times \left({}^{t+\Delta t}_{0}I_3\right)^{-\frac{1}{3}}\left(\delta_{ij} - \frac{1}{3}\,{}^{t+\Delta t}_{0}I_1\ {}^{t+\Delta t}_{0}G^{-1}_{ij}\right)\Bigg\} \\ &\quad + k\,{}^{t+\Delta t}_{0}J\left({}^{t+\Delta t}_{0}J - 1\right){}^{t+\Delta t}_{0}G^{-1}_{ij} \end{aligned} \tag{5}$$

To solve this nonlinear equation, the linearized incremental form of the equilibrium equation is introduced over the time interval $[t, t+\Delta t]$ as

$$\begin{aligned} a^*\left({}^{t}_{0}z; {}_0z, {}_0\bar{z}\right) &\equiv \int_{0_\Omega} {}^{t}_{0}W_{,\varepsilon_{ij},\,\varepsilon_{rs}}\ {}_0e_{rs}\ {}_0\bar{e}_{ij}\ {}^{0}\mathrm{d}\Omega + \int_{0_\Omega} {}^{t}_{0}W_{,\varepsilon_{ij}}\ {}_0\bar{\eta}_{ij}\ {}^{0}\mathrm{d}\Omega \\ &= \int_{0_\Omega} {}_0D_{ijrs}\left({}_0z_{r,s} + {}^{t}_{0}z_{k,r}\ {}_0z_{k,s}\right)\left(\bar{z}_{i,j} + {}^{t}_{0}z_{\ell,i}\ {}_0\bar{z}_{\ell,j}\right){}^{0}\mathrm{d}\Omega \\ &\quad + \int_{0_\Omega} {}^{t}_{0}W_{,\varepsilon_{ij}}\ {}_0z_{k,i}\ {}_0\bar{z}_{k,j}\ {}^{0}\mathrm{d}\Omega = \ell({}_0\bar{z}) - \int_{0_\Omega} {}^{t}_{0}W_{,\varepsilon_{ij}}\ {}_0\bar{e}_{ij}\ {}^{0}\mathrm{d}\Omega \\ &= \ell({}_0\bar{z}) - a\left({}^{t}_{0}z, {}_0\bar{z}\right) \end{aligned} \tag{6}$$

Note that in Eq. (6) the external load is assumed to be deformation independent. The energy bilinear form $a^*({}^{t}_{0}z; {}_0z, {}_0\bar{z})$ is linear in both the displacement increment ${}_0z$ and virtual displacement ${}_0\bar{z}$. Increments in stress are computed using the constitutive law, ${}_0S_{ij} = {}_0D_{ijrs}\ {}_0\varepsilon_{rs}$, where $\boldsymbol{D}$ is the fourth-order incremental strain-stress tensor.[22]

III. Reproducing Kernel Particle Method

A. Construction of a Kernel Function

The RKPM discretization is based on the following kernel estimation of a function[5]:

$$z^R(x) = \int_{\Omega_x} \Phi_a(x-s)z(s)\,\mathrm{d}s \tag{7}$$

where

$$\Phi_a(x-s) = (1/a)\Phi[(x-s)/a] \tag{8}$$

The term $z^R(x)$ is the reproduced $z(x)$, $\Phi_a(x-s)$ is the kernel function, and a is the dilation parameter that controls the size of the support of $\Phi_a(x-s)$. For nonnegative $\Phi_a(x-s)$ with the integral normalized to unity, $z^R(x)$ converges to $z(x)$ as $a \to 0$. If the kernel function is the Dirac delta function, $z^R(x)$ reproduces $z(x)$ exactly. In computation, functions such as Gaussian or spline functions with small supports are usually used as kernel functions. In this work, the following cubic spline is used (see Fig. 1):

$$\Phi(\alpha) = \begin{cases} \frac{2}{3} - 4|\alpha|^2 + 4|\alpha|^3, & \text{for} \quad 0 \le |\alpha| \le \frac{1}{2} \\ \frac{4}{3} - 4|\alpha| + 4|\alpha|^2 - \frac{4}{3}|\alpha|^3, & \text{for} \quad \frac{1}{2} < |\alpha| \le 1 \\ 0, & \text{for} \quad |\alpha| > 1 \end{cases} \tag{9}$$

Equation (7) is the foundation of SPH.[1] Liu et al.[5] suggested a modification of Eq. (7) to improve the accuracy of SPH by

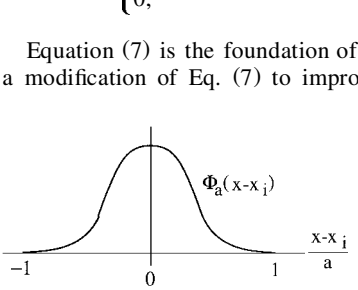

Fig. 1 Cubic spline kernel function.

introducing a modified kernel function such that the kernel estimation exactly reproduces polynomials:

$$z^R(x) = \int_{\Omega_x} \bar{\Phi}_a(x; x-s) z(s)\, \mathrm{d}s \tag{10}$$

where

$$\bar{\Phi}_a(x; x-s) = \Phi_a(x-s) C(x; x-s) \tag{11}$$

is the modified kernel function. In Eq. (11), $C(x; x-s)$ is called the correction function and is expressed by an Nth-order polynomial of $(x-s)$, i.e.,

$$C(x; x-s) = \sum_{i=0}^{N} b_i(x)(x-s)^i \equiv \boldsymbol{H}^T(x-s)\boldsymbol{b}(x) \tag{12}$$

where

$$\boldsymbol{H}^T(x-s) = [1, x-s, (x-s)^2, \ldots, (x-s)^N] \tag{13}$$

and

$$\boldsymbol{b}^T(x) = [b_0(x), b_1(x), \ldots, b_N(x)] \tag{14}$$

and the various $b_i(x)$ are functions of x. The coefficient vector $\boldsymbol{b}(x)$ is determined by satisfying the condition that, if $z(x)$ is a polynomial of degree at most N, then $z^R(x) = z(x)$.

Expressing an Nth-order polynomial of $z(s)$ in terms of power series of $(s-x)$ by a Taylor expansion, the imposition of $z^R(x) = z(x)$ leads to the following equations:

$$\bar{m}_n = \delta_{n0}, \qquad n = 0, 1, \ldots, N \tag{15}$$

where

$$\bar{m}_n(x) = \int_{\Omega_x} (x-s)^n C(x; x-s) \Phi_a(x-s)\, \mathrm{d}s$$

$$= \sum_{k=0}^{N} b_k(x) m_{n+k}(x) \tag{16}$$

and

$$m_n(x) = \int_{\Omega_x} (x-s)^n \Phi_a(x-s)\, \mathrm{d}s \tag{17}$$

Equations given in Eq. (15) are called the reproducing conditions.[5,6] By rearranging Eqs. (15–17), $\boldsymbol{b}(x)$ can be obtained from

$$\boldsymbol{b}(x) = \boldsymbol{M}^{-1}(x)\boldsymbol{H}(0) \tag{18}$$

where the moment matrix is introduced as

$$\boldsymbol{M}_{IJ}(x) = m_{I+J}(x) = \int_{\Omega_x} (x-s)^{I+J} \Phi_a(x-s)\, \mathrm{d}s \tag{19}$$

Finally, the modified kernel function $\bar{\Phi}_a(x; x-s)$ is obtained by

$$\bar{\Phi}_a(x; x-s) = \Phi_a(x-s) C(x; x-s)$$

$$= \Phi_a(x-s)\, \boldsymbol{H}^T(x-s)\, \boldsymbol{M}^{-1}(x)\, \boldsymbol{H}(0) \tag{20}$$

The discretized reproducing equation is obtained by performing numerical integration of Eq. (10). An example of discretization is employing the trapezoidal rule to the reproducing equation to yield

$$z^R(x) \cong \sum_{i=1}^{\mathrm{NP}} \bar{\Phi}_a(x; x-x_i) z(x_i) \Delta x_i \equiv \sum_{i=1}^{\mathrm{NP}} \Psi_i(x) z_i \tag{21}$$

where NP is the total number of particles and

$$\Psi_i(x) = \bar{\Phi}_a(x; x-x_i) \Delta x_i \tag{22}$$

can be interpreted as the interpolation functions of $z^R(x)$. The derivative of the interpolation function $\Psi_i(x)$ is obtained using

$$\bar{\Phi}_{a,x}(x; x-x_i) = \Phi_{a,x}(x-x_i)\, \boldsymbol{H}^T(x-x_i)\, \boldsymbol{M}^{-1}(x)\, \boldsymbol{H}(0)$$

$$+ \Phi_a(x-x_i)\, \boldsymbol{H}^T_{,x}(x-x_i)\, \boldsymbol{M}^{-1}(x)\, \boldsymbol{H}(0)$$

$$+ \Phi_a(x-x_i)\, \boldsymbol{H}^T(x-x_i)\, \boldsymbol{M}^{-1}_{,x}(x)\, \boldsymbol{H}(0) \tag{23}$$

and

$$\boldsymbol{M}^{-1}_{,x}(x) = -\boldsymbol{M}^{-1}(x)\, \boldsymbol{M}_{,x}(x)\, \boldsymbol{M}^{-1}(x) \tag{24}$$

Several remarks were discussed in Ref. 7 and are repeated here.

1) The term $\boldsymbol{M}$ is the Gram matrix of a set of basis functions $\{1, x-s, (x-s)^2, \ldots, (x-s)^N\}$ with respect to Φ_a. Because Φ_a is chosen to be a positive function, $\boldsymbol{M}$ is nonsingular.

2) If $z(x)$ is an Nth-order polynomial, the reproducing Eq. (10) reproduces $z(x)$ exactly.

3) The matrix $\boldsymbol{M}$ and its derivatives need to be integrated using the same integration rule as in Eq. (21).

4) The smoothness of the interpolation function $\Psi_I(x)$ depends greatly on the smoothness of the kernel function Φ_a. It was discussed in Ref. 8 that, if $\Phi_a \in C^m(\Omega_x)$, then $\Psi_i(x) \in C^m(\Omega_x)$.

5) In the case where the support of $\Phi_a(x-x_i)$ does not intersect with the boundary, $\boldsymbol{M}$ degenerates to a constant matrix if particles are equally spaced, and the trapezoidal rule is used for integration.

6) The support of the kernel function has to cover at least one adjacent point to maintain numerical stability (which is often referred to as the kernel stability).

7) The shape function $\Psi_i(x)$ does not possess Kronecker delta properties, i.e., $\Psi_i(x_j) \neq \delta_{ij}$. The extension of Φ_a to multidimensional cases is straightforward and can be found in Ref. 8.

B. RKPM Galerkin Approximation

Let $\boldsymbol{z}^h$ and $\bar{\boldsymbol{z}}^h$ be RKPM approximations of $\boldsymbol{z}$ and $\bar{\boldsymbol{z}}$, respectively. Using the Galerkin approximation, the problem statement is as follows. For a structure with domain ${}^0\Omega$ and boundary ${}^0\Gamma$ (a subset of which ${}^0\Gamma_g$ is an essential boundary with prescribed displacement $\boldsymbol{g}$), given the energy density function W, body forces $\boldsymbol{f}$, and traction forces $\boldsymbol{T}$, find $\boldsymbol{z}^h \in {}_0Z_g \subset H^1_g = [z: z \in H^1({}^0\Omega), z_i = g_i \text{ on } {}^0\Gamma_g]$, such that for all $\boldsymbol{z}^h \in {}_0Z \subset H^1_0 = [z: z \in H^1({}^0\Omega), z_i = 0 \text{ on } {}^0\Gamma_g]$,

$$a\left({}^{t+\Delta t}\boldsymbol{z}^h, {}_0\bar{\boldsymbol{z}}^h\right) = \int_{{}^0\Omega} {}^{t+\Delta t}_0 S_{ij} \left({}^{t+\Delta t}\boldsymbol{z}^h\right) {}^{t+\Delta t}_0 \bar{\varepsilon}_{ij}\left({}_0\bar{\boldsymbol{z}}^h\right) {}^0\mathrm{d}\Omega$$

$$= \int_{{}^0\Omega} {}^{t+\Delta t}_0 f_i\ {}_0\bar{z}^h_i\, {}^0\mathrm{d}\Omega + \int_{{}^0\Gamma} {}^{t+\Delta t}_0 T_i\ {}_0\bar{z}^h_i\, {}^0\mathrm{d}\Gamma = \mathscr{L}\left({}_0\bar{\boldsymbol{z}}^h\right) \tag{25}$$

The RKPM interpolation functions for ith components of $\boldsymbol{z}^h$ and $\bar{\boldsymbol{z}}^h$ are

$$z^h_i(\boldsymbol{x}) = \sum_{I=1}^{\mathrm{NP}} \Psi_I(\boldsymbol{x})\, d_{iI} \tag{26}$$

and

$$\bar{z}^h_i(\boldsymbol{x}) = \sum_{I=1}^{\mathrm{NP}} \Psi_I(\boldsymbol{x})\, \bar{d}_{iI} \tag{27}$$

where d_{iI} and $\bar{d}_{iI}$ are the ith components of the generalized displacement and generalized virtual displacement of particle I, respectively.

Because $\Psi_I(\boldsymbol{x})$ does not hold Kronecker delta properties, essential boundary conditions cannot be introduced directly. Chen et al.[7,8] proposed a direct transformation method where generalized displacements are transformed to nodal displacements $\hat{d}_{iI}$ by

$$\hat{d}_{iI} = \sum_{J=1}^{\mathrm{NP}} A_{JI}\, d_{iJ} \tag{28}$$

where

$$A_{IJ} = \Psi_I(\boldsymbol{x}_J) \tag{29}$$

The displacements are then interpolated by

$$z^h_i(\boldsymbol{x}) = \sum_{K=1}^{\mathrm{NP}} \hat{\Psi}_K(\boldsymbol{x}) \hat{d}_{iK} \tag{30}$$

where

$$\hat{\Psi}_K(\boldsymbol{x}) = \sum_{I=1}^{\mathrm{NP}} A^{-1}_{KI}\, \Psi_I(\boldsymbol{x}) \tag{31}$$

With this newly defined interpolation function $\hat{\Psi}_K(\boldsymbol{x})$, essential boundary conditions are imposed by

$$\left.\begin{aligned}\hat{d}_{iI} &= g_i(\boldsymbol{x}_J)\\ \bar{\hat{d}}_{iI} &= 0\end{aligned}\right\}, \qquad \text{for} \qquad \boldsymbol{x}_J \in {}^0\Gamma_g \tag{32}$$

Note that, in computational implementation, the stiffness matrix and force vectors are formed using $\Psi_I(\boldsymbol{x})$ and then transformed to the nodal coordinate system by the transformation matrix $\boldsymbol{A}$, defined by Eq. (29). The resulting discretized RKPM incremental equilibrium equation is similar to that of the FEM, except that no explicit mesh is needed to construct shape functions.

For large deformation analysis, a material RKPM kernel function was introduced in Refs. 7 and 8 so that the kernel function covers the same set of material particles throughout the course of deformation. This formulation ensures that the kernel stability condition is satisfied regardless of the material distortion. This method expresses the kernel function in original configuration in the following form:

$$\Phi_a\left({}^0\boldsymbol{x} - {}^0\boldsymbol{x}_I\right) = \frac{1}{a}\Phi\left(\frac{\left\|{}^0\boldsymbol{x} - {}^0\boldsymbol{x}_I\right\|}{a}\right) \tag{33}$$

where ${}^0\boldsymbol{x}$ is the material coordinate. Although this material kernel function fits naturally for the total Lagrangian formulation, it can also be used for the updated Lagrangian formulation in which the spatial derivative is obtained by the chain rule

$$\frac{\partial \Phi_a\left({}^0\boldsymbol{x} - {}^0\boldsymbol{x}_I\right)}{\partial\, {}^t x_i} = \frac{\partial \Phi_a\left({}^0\boldsymbol{x} - {}^0\boldsymbol{x}_I\right)}{\partial\, {}^0 x_i}\, {}^t_0F^{-1}_{ij} \tag{34}$$

IV. Material Design Sensitivity Analysis

Consider a structural system in the final equilibrium configuration at time t (instead of $t+\Delta t$ of Sec. II), corresponding to a given material property design variable u. Using Eq. (4), we can write the equilibrium equation for the structural system as

$$a_u\left({}^t_0z,\ {}_0\bar{z}\right) = \ell_u({}_0\bar{z}), \qquad \text{for all} \qquad {}_0\bar{z} \in {}_0Z \tag{35}$$

When the material property is perturbed to $u+\tau\delta u$, the structure reaches another equilibrium configuration at time $t+\Delta t$. The new equation of equilibrium is

$$a_{u+\tau\delta u}\left[{}^{t+\Delta t}_0z(u+\tau\delta u),\ {}_0\bar{z}\right] = \ell_{u+\tau\delta u}({}_0\bar{z}), \qquad \text{for all} \qquad {}_0\bar{z} \in {}_0Z \tag{36}$$

The variation of the solution ${}^tz$ of Eq. (35) with respect to material property u is defined as[10]

$${}_0z' \equiv \frac{\mathrm{d}}{\mathrm{d}\tau}\,{}^{t+\Delta t}_0z(u+\tau\delta u)\bigg|_{\tau=0} = \lim_{\tau\to 0}\frac{{}^{t+\Delta t}_0z(u+\tau\delta u) - {}^t_0z(u)}{\tau} \tag{37}$$

The first-order variation of the energy form with respect to the material property u is[10]

$$\begin{aligned}&\frac{\mathrm{d}}{\mathrm{d}\tau}\left\{a_{u+\tau\delta u}\left[{}^{t+\Delta t}_0z(u+\tau\delta u),\ {}_0\bar{z}\right]\right\}_{\tau=0}\\ &\quad\equiv a'_{\delta u}\left({}^t_0z,\ {}_0\bar{z}\right) + a^*_u\left({}^t_0z;\, {}_0z',\, {}_0\bar{z}\right)\end{aligned} \tag{38}$$

where $a'_{\delta u}$ is the first-order variation of the energy form of Eq. (36) with respect to its explicit dependence on the material property u:

$$a'_{\delta u}\left({}^tz,\ {}_0\bar{z}\right) \equiv \frac{\mathrm{d}}{\mathrm{d}\tau}\left[a_{u+\tau\delta u}\left({}^{t+\Delta t}\tilde{z},\ {}_0\bar{z}\right)\right]_{\tau=0} \tag{39}$$

The tilde indicates a variable that is to be held constant for the process of partial differentiation. The first-order variation of the load form of Eq. (36) is

$$\ell_{\delta u}({}_0\bar{z}) \equiv \frac{\mathrm{d}}{\mathrm{d}\tau}\left[\ell_{u+\tau\delta u}({}_0\bar{z})\right]_{\tau=0} \tag{40}$$

The sensitivity equation of the direct differentiation method is obtained then as

$$a^*_u\left({}^t_0z;\, {}_0z',\ {}_0\bar{z}\right) = \ell_{\delta u}({}_0\bar{z}) - a'_{\delta u}\left({}^t_0z,\ {}_0\bar{z}\right), \quad \text{for all} \quad {}_0\bar{z} \in {}_0Z \tag{41}$$

Note that the same energy bilinear form appears on the left-hand sides of Eqs. (6) and (41). Correspondingly, the stiffness matrices will be identical when the two equations are discretized, leading to a very efficient calculation of the sensitivity coefficients.

The second term on the right-hand side of Eq. (41) is

$$a'_{\delta u}\left({}^t_0z,\ {}_0\bar{z}\right) = \int\!\!\int_{{}^0\Omega}\left({}^t_0S_{ij}\right)'\,{}_0\bar{\varepsilon}_{ij}\,{}^0\mathrm{d}\Omega \tag{42}$$

where Eq. (5) is used to compute the variation of stress components with respect to material property u as

$$\begin{aligned}\left({}^t_0S_{ij}\right)' = 2\Big\{&\left[A'_{10} + 2A'_{20}\left({}^t_0\hat{I}_1 - 3\right) + 3A'_{30}\left({}^t_0\hat{I}_1 - 3\right)^2\right]\\ &\times\left({}^t_0I_3\right)^{-\frac{1}{3}}\left(\delta_{ij} - \tfrac{1}{3}\,{}^t_0I_1\,{}^t_0C^{-1}_{ij}\right)\Big\} + K'\,{}^t_0J\left({}^t_0J - 1\right){}^t_0C^{-1}_{ij}\end{aligned} \tag{43}$$

For the total Lagrangian formulation, we can write a general structural performance measure at the final equilibrium configuration $t+\Delta t$ corresponding to perturbed design $u+\tau\delta u$ as

$${}^{t+\Delta t}_0\psi = \int_{{}^0\Omega} g\left({}^{t+\Delta t}_0z,\ {}_0\nabla\,{}^{t+\Delta t}_0z,\, u+\tau\delta u\right){}^0\mathrm{d}\Omega \tag{44}$$

The first-order variation of the performance measure with respect to the material property design variable is obtained as[10]

$$\begin{aligned}{}^t_0\psi' &\equiv \frac{\mathrm{d}}{\mathrm{d}\tau}\left[\int_{{}^0\Omega} g\left({}^t_0z,\ {}_0\nabla\,{}^tz,\, u+\tau\delta u\right){}^0\mathrm{d}\Omega\right]_{\tau=0}\\ &= \int_{{}^0\Omega}\left(g,_{{}^t_0z}\,{}_0z' + g,_{{}_0\nabla\,{}^tz}\,{}_0\nabla z' + g,_u\,\delta u\right){}^0\mathrm{d}\Omega\end{aligned} \tag{45}$$

Once ${}^t_0z$ and ${}_0z'$ are obtained from Eqs. (6) and (41), respectively, ${}^t_0\psi'$ can be obtained from Eq. (45).

For the adjoint variable method, an adjoint equation is introduced as[10]

$$a^*_u\left({}^t_0z;\, {}_0\lambda,\, {}_0\bar{\lambda}\right) = \int_{{}^0\Omega}\left(g,_{{}^t_0z}\,{}_0\bar{\lambda} + g,_{{}_0\nabla\,{}^tz}\,{}_0\nabla\,{}_0\bar{\lambda}\right){}^0\mathrm{d}\Omega \qquad \text{for all} \qquad {}_0\bar{\lambda} \in {}_0Z \tag{46}$$

Solving Eq. (46) to obtain the adjoint variable ${}_0\lambda$, design sensitivities ${}^t_0\psi'$ can be computed using

$${}^t_0\psi' = \int_{{}^0\Omega} g,_u\,\delta u\,{}^0\mathrm{d}\Omega + \ell_{\delta u}({}_0\lambda) - a'_{\delta u}\left({}^t_0z,\ {}_0\lambda\right) \tag{47}$$

A complete derivation is given in Ref. 10.

V. Shape Design Sensitivity Analysis

In shape DSA, parameters that determine the geometric shape of the structural domain are treated as design variables. The relationship between shape variation of a continuous domain and the resulting variation in structural performance measures can be described using the material derivative of continuum mechanics.[18]

A. Design Velocity Field

Consider a structural domain ${}^0\Omega$ with its boundary ${}^0\Gamma$ as a continuous medium at the initial design $\tau=0$ shown in Fig. 2 (solid lines). Suppose only one parameter τ defines the transformation $\boldsymbol{T}$ that changes the structural domain from ${}^0\Omega$ to ${}^0\Omega_\tau$ (dotted lines). The transformation mapping $\boldsymbol{T}$ that represents this process can be defined as

$$\boldsymbol{T}: {}^0\boldsymbol{x} \to {}^0\boldsymbol{x}_\tau({}^0\boldsymbol{x}) \qquad \text{for} \qquad {}^0\boldsymbol{x} \in {}^0\Omega \tag{48}$$

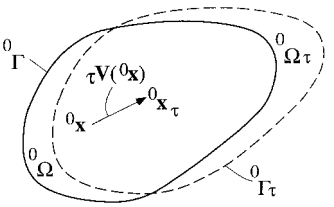

Fig. 2 Shape change process.

Define the design velocity field $\boldsymbol{V}$, with τ playing the role of (design) time, as[18]

$$\boldsymbol{V}\left({}^0\boldsymbol{x}_\tau,\,\tau\right) \equiv \frac{\mathrm{d}^0\boldsymbol{x}_\tau}{\mathrm{d}\tau} = \frac{\mathrm{d}\boldsymbol{T}\left({}^0\boldsymbol{x}_\tau,\,\tau\right)}{\mathrm{d}\tau} = \frac{\partial \boldsymbol{T}\left({}^0\boldsymbol{x}_\tau,\,\tau\right)}{\partial\tau} \tag{49}$$

In the neighborhood of initial time $\tau = 0$, assuming a regularity hypothesis and ignoring higher-order terms, $\boldsymbol{T}$ can be approximated by

$$\boldsymbol{T}({}^0\boldsymbol{x},\,\tau) = \boldsymbol{T}({}^0\boldsymbol{x},\,0) + \tau\frac{\partial \boldsymbol{T}({}^0\boldsymbol{x}_\tau,\,\tau)}{\partial\tau} + \mathcal{O}(\tau^2) \cong {}^0\boldsymbol{x} + \tau\boldsymbol{V}({}^0\boldsymbol{x}) \tag{50}$$

where ${}^0\boldsymbol{x} \equiv \boldsymbol{T}({}^0\boldsymbol{x},\,0)$ and $\boldsymbol{V}({}^0\boldsymbol{x}) \equiv \boldsymbol{V}({}^0\boldsymbol{x},\,0)$.

B. Design Sensitivity Analysis

Consider a structural system in its final equilibrium configuration, at time t, instead of $t+\Delta t$ as in Sec. II, corresponding to the initial domain ${}^0\Omega$ at $\tau = 0$. The equilibrium equation of the structural system is of the form

$$a_{0_\Omega}\left({}^t_0z,\,{}_0\bar{z}\right) \equiv \int_{0_\Omega} {}^t_0S_{ij}\,{}^t_0\bar{\varepsilon}_{ij}\,\mathrm{d}\Omega = \int_{0_\Omega} {}^t_0f_i\,{}_0\bar{z}_i\,\mathrm{d}\Omega + \int_{0_\Gamma} {}^t_0T_i\,{}_0\bar{z}_i\,\mathrm{d}\Gamma$$
$$\equiv \ell_{0_\Omega}({}_0\bar{z}), \qquad \text{for all} \qquad {}_0\bar{z} \in {}_0Z \tag{51}$$

Using the total Lagrangian formulation, the variational equation of equilibrium on a perturbed domain ${}^0\Omega_\tau$ at its final equilibrium configuration time $t+\Delta t$ is[15]

$$a_{0_{\Omega_\tau}}\left({}^{t+\Delta t}_0z,\,{}_0\bar{z}\right) = \ell_{0_{\Omega_\tau}}({}_0\bar{z}), \qquad \text{for all} \qquad {}_0\bar{z} \in {}_0Z_\tau \tag{52}$$

The pointwise total material derivative of the structural responses ${}^{t+\Delta t}_0z({}^0\boldsymbol{x}_\tau)$ is[15]

$${}_0\dot{z}({}^0\boldsymbol{x}) = \lim_{\tau\to 0}\frac{{}^{t+\Delta t}_0z[{}^0\boldsymbol{x}+\tau\boldsymbol{V}({}^0\boldsymbol{x})] - {}^t_0z({}^0\boldsymbol{x})}{\tau}$$
$$\equiv {}_0z'({}^0\boldsymbol{x}) + {}_0\nabla\,{}^tz^T\boldsymbol{V}({}^0\boldsymbol{x}) \tag{53}$$

Taking the total material derivative on both sides of Eq. (52) and using Lemmas 3.2.1 and 3.2.2 from Ref. 18, one obtains

$$\left[a_{0_\Omega}\left({}^t_0z,\,{}_0\bar{z}\right)\right]' \equiv a^*_{0_\Omega}\left({}^t_0z;\,{}_0\dot{z},\,{}_0\bar{z}\right) + a'_V\left({}^t_0z,\,{}_0\bar{z}\right)$$
$$= \ell_V({}_0\bar{z}), \qquad \text{for all} \qquad {}_0\bar{z} \in {}_0Z \tag{54}$$

where[15]

$$a'_V\left({}^t_0z,\,{}_0\bar{z}\right) = -a^*_{0_\Omega}\left({}^t_0z;\,{}_0\nabla\,{}^tz^T\boldsymbol{V},\,{}_0\bar{z}\right)$$
$$- a_{0_\Omega}\left({}^t_0z,\,{}_0\nabla{}^t\bar{z}^T\boldsymbol{V}\right) + \hat{a}_{0_\Omega}\left({}^t_0z,\,{}_0\bar{z}\right) \tag{55}$$

and

$$\hat{a}_{0_\Omega}\left({}^t_0z,\,{}_0\bar{z}\right) = \int_{0_\Omega}\left(\nabla\left[{}^t_0S_{ij}\,{}^t_0\bar{\varepsilon}_{ij}\right]^T\boldsymbol{V} + {}^t_0S_{ij}\,{}^t_0\bar{\varepsilon}_{ij}\,\mathrm{div}\,\boldsymbol{V}\right){}^0\mathrm{d}\Omega \tag{56}$$

We can rewrite Eq. (54) as

$$a^*_{0_\Omega}\left({}^t_0z;\,{}_0\dot{z},\,{}_0\bar{z}\right) = \ell_V({}_0\bar{z}) - a'_V\left({}^t_0z,\,{}_0\bar{z}\right), \qquad \text{for all} \qquad {}_0\bar{z} \in {}_0Z \tag{57}$$

This is the sensitivity equation that has to be solved for the total derivative of the structural response. The left-hand side of Eq. (57) exhibits the same bilinear form as Eq. (6), and so the computation of sensitivity coefficients is very efficient.

Consider a general structural performance measure in an integral form as

$${}^{t+\Delta t}_0\psi = \int_{0_{\Omega_\tau}} g\left({}^{t+\Delta t}_0z,\,{}_0\nabla\,{}^{t+\Delta t}_0z\right){}^0\mathrm{d}\Omega_\tau \tag{58}$$

The first-order variation of the performance measure with respect to the shape design variable using total material derivative is[15]

$${}^t_0\psi' = \int_{0_\Omega}\left[g,_{{}^t_0z}\,{}_0\dot{z} + g,_{{}_0\nabla\,{}^tz}\,{}_0\nabla\dot{z} + g,_{{}_0\nabla\,{}^tz}\,{}_0\nabla\left({}_0\nabla\,{}^tz^T\right)\boldsymbol{V}\right.$$
$$\left. - g,_{{}_0\nabla\,{}^tz}\,{}_0\nabla\left({}_0\nabla\,{}^tz^T\boldsymbol{V}\right) + {}_0\nabla g^T\boldsymbol{V} + g\,\mathrm{div}\,\boldsymbol{V}\right]{}^0\mathrm{d}\Omega \tag{59}$$

Once ${}^t_0z$ and ${}_0\dot{z}$ are obtained from Eqs. (6) and (57), respectively, ${}^t_0\psi'$ can be obtained from Eq. (59). This is the direct differentiation method. Design velocity field $\boldsymbol{V}$ must be computed carefully so that it satisfies theoretical and practical requirements.[27]

For the adjoint variable method, an adjoint equation is introduced as[15]

$$a^*_u\left({}^t_0z;\,{}_0\lambda,\,{}_0\bar{\lambda}\right) = \int_{0_\Omega}\left(g,_{{}^t_0z}\,{}_0\bar{\lambda} + g,_{{}_0\nabla\,{}^tz}\,{}_0\nabla\,{}_0\bar{\lambda}\right){}^0\mathrm{d}\Omega$$
$$\text{for all} \qquad {}_0\bar{\lambda} \in {}_0Z \tag{60}$$

Solving Eq. (60) for the adjoint variable ${}_0\lambda$, the design sensitivity ${}^t_0\psi'$ can be computed using

$${}^t_0\psi' = \mathcal{L}_V({}_0\lambda) - a'_V\left({}^t_0z,\,{}_0\lambda\right) + \int_{0_\Omega}\left[g,_{{}_0\nabla\,{}^tz}\,{}_0\nabla\left({}_0\nabla\,{}^tz^T\right)\boldsymbol{V}\right.$$
$$\left. - g,_{{}_0\nabla\,{}^tz}\,{}_0\nabla\left({}_0\nabla\,{}^tz^T\boldsymbol{V}\right) + {}_0\nabla g^T\boldsymbol{V} + g\,\mathrm{div}\,\boldsymbol{V}\right]{}^0\mathrm{d}\Omega \tag{61}$$

A complete derivation is given in Ref. 15.

VI. Numerical Implementation

In this section, the computational procedure for proposed DSA is presented. We employ a computational algorithm for a fictitious load for the material DSA to explain the procedure.

A. Computational Procedure of DSA

The computational procedure shown in Fig. 3 has been implemented for material and shape DSA using RKPM. Here, an RKPM code is used to obtain structural responses at the final configuration ${}^t_0z$. The fictitious and adjoint loads are evaluated externally to the RKPM code, using the direct differentiation method [Eq. (41) for material design variables and Eq. (57) for shape design variables] or the adjoint variable method [Eqs. (46) and (60)]. Then these loads are considered as additional loading cases to solve for ${}_0z'$ or ${}_0\dot{z}$ or ${}_0\boldsymbol{\lambda}$, using the tangent stiffness matrix that has been decomposed at the last iteration for time t of the original structural analysis. The final step is to compute ${}^t_0\psi'$ using the direct differentiation method [Eq. (45) for material and Eq. (59) for shape] or the adjoint variable method [Eq. (47) for material and Eq. (61) for shape]. Note that the same interpolation functions used in RKPM, i.e., Eq. (31), are used to interpolate structural responses at integration points for the computation of adjoint loads, fictitious loads, and sensitivity expressions.

Shape DSA requires special attention while using the RKPM method because the shape functions for a particle depend on the

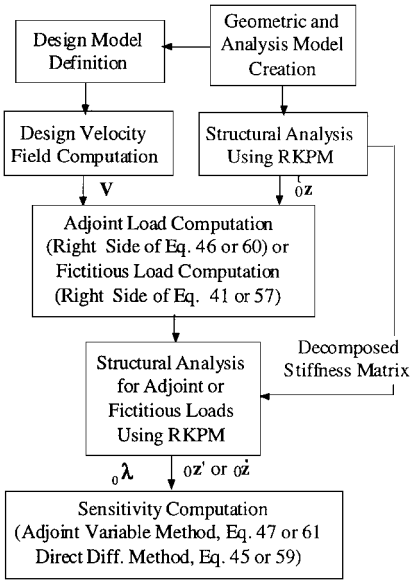

Fig. 3 DSA computational procedure.

positions of its neighboring particles. Shape changes influence the interpolation functions due to movement of neighboring particles. From Eqs. (26) and (27) it follows that

$$\dot{z}_i^h(\boldsymbol{x}) = \sum_{I=1}^{\mathrm{NP}} \Psi_I(\boldsymbol{x})\, \dot{d}_{iI} + \sum_{I=1}^{\mathrm{NP}} \dot{\Psi}_I(\boldsymbol{x})\, d_{iI} \tag{62}$$

$$\dot{\bar{z}}_i^h(\boldsymbol{x}) = \sum_{I=1}^{\mathrm{NP}} \Psi_I(\boldsymbol{x})\, \dot{\bar{d}}_{iI} + \sum_{I=1}^{\mathrm{NP}} \dot{\Psi}_I(\boldsymbol{x}) \bar{d}_{iI} \tag{63}$$

where $\dot{\Psi}_I(\boldsymbol{x})$ is the total derivative of the interpolation function with respect to shape design parameter. Because

$$\sum_{I=1}^{\mathrm{NP}} \Psi_I(\boldsymbol{x})\, \dot{\bar{d}}_{iI} \in {}_0Z^h$$

the path $\dot{\bar{d}}_{iI} = 0$ can be selected to simplify the formula. Note that in the discretized form $\dot{\bar{z}}_i^h(\boldsymbol{x}) \neq 0$.

B. Computational Algorithm

The computational algorithm for the fictitious load of material DSA, Eq. (41), is listed next to explain the computational procedure. Similar algorithms were developed to support computation of adjoint loads and sensitivity expressions for material and shape design variables. In this algorithm, ${}^{0}_{x}\Omega^I$ is the domain of support of the interpolation function $\Psi_I({}^0\boldsymbol{x})$ associated with the particle I with position vector ${}^0\boldsymbol{x}_I$; $S^A = \{{}^0\boldsymbol{x}_I : {}^0\boldsymbol{x}_A \in {}^{0}_{x}\Omega^I\}$ is a set of particles in which the domain of support associated with each particle covers ${}^0\boldsymbol{x}_A$; and NA is the number of particles in set S^A. Figure 4 illustrates an RKPM discretization, where $S^A = \{{}^0\boldsymbol{x}_I, {}^0\boldsymbol{x}_J, {}^0\boldsymbol{x}_K\}$ and NA = 3.

The computational algorithm using the Gauss integration is as follows:

Loop over integration zones
  Loop over Gauss integration points ${}^0\boldsymbol{x}_A$
    Loop over all particles ${}^0\boldsymbol{x}_I \in S^A$
      Compute the interpolation function $\Psi_I({}^0\boldsymbol{x}_A)$
      Compute the derivatives of interpolation function $\Psi_{I,i}({}^0\boldsymbol{x}_A)$ with respect to the ith coordinate
    End loop over particles ${}^0\boldsymbol{x}_I \in S^A$
    Compute deformation gradient ${}^t_0\boldsymbol{F}({}^0\boldsymbol{x}_A)$; use the deformation gradient at ${}^0\boldsymbol{x}_A$ to evaluate
      Green–Lagrange strain tensor ${}^t_0\varepsilon$
      Variation of the second Piola–Kirchhoff stress tensor with respect to material design variables, i.e., Eq. (43)
    Loop over neighboring particles ${}^0\boldsymbol{x}_J \in S^A$ to
      Compute fictitious loads corresponding to each particle using the right-hand side of Eq. (41)
      Assemble fictitious loads at particles to generate a global fictitious load vector $\boldsymbol{f}$ at the generalized coordinates
    End loop over particles ${}^0\boldsymbol{x}_J \in S^A$
  End loop over integration points ${}^0\boldsymbol{x}_A$
End loop over integration zones

Transform the global fictitious load vector from the generalized coordinates to the nodal coordinates, using

$$\hat{f}_{iI} = \sum_{J=1}^{\mathrm{NP}} A_{JI}^{-1} f_{iJ}$$

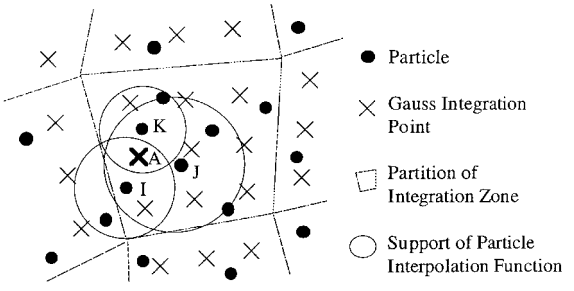

Fig. 4 RKPM discretization.

VII. Examples

An infinitely long rubber tube (modeled as both one- and two-dimensional problems), a two-dimensional rectangular rubber band, and an engine mount are presented in this section to demonstrate the proposed DSA method. In this paper, the linear function $\boldsymbol{H} = [1, x - s]$ and the quadrature rules of Ref. 8 are used.

A. Infinitely Long Rubber Tube

An infinitely long rubber tube with an internal pressure P is modeled as both one- and two-dimensional axisymmetric problems, as shown in Fig. 5. Inner and outer radii of the tube are 60 and 80 mm, respectively. The pressure P is 0.5 MPa. Analysis results of this problem have been verified using an analytical solution.[26] The variational equilibrium equation of the two-dimensional axisymmetric problem using the total Lagrangian formulation is

$$a_u({}^t_0\boldsymbol{z}, {}_0\bar{\boldsymbol{z}}) \equiv \int_{{}^0_\Omega} \left({}^t_0S_{ij}\, {}^t_0\bar{\varepsilon}_{ij} + {}^t_0S_{33}\, {}^t_0\bar{\varepsilon}_{33} \right) {}^0x_1\, {}^0\mathrm{d}\Omega$$

$$= \int_{{}^0_\Gamma} P\, {}^t_0x_1\, {}_0\bar{z}\, {}^0\mathrm{d}\Gamma \equiv \ell_u({}_0\bar{\boldsymbol{z}}), \quad \text{for all} \quad {}_0\bar{\boldsymbol{z}} \in {}_0Z \tag{64}$$

where ${}^t_0S_{ij}$ is defined in Eq. (5) and the strains are

$${}^t_0\varepsilon_{ij} = {}^t_0e_{ij} + {}^t_0\eta_{ij} = \tfrac{1}{2}\left({}^t_0z_{i,j} + {}^t_0z_{i,j}\right) + \tfrac{1}{2}\left({}^t_0z_{k,i}\, {}^t_0z_{k,j}\right), \quad \text{for} \quad i, j, k = 1, 2 \tag{65a}$$

$${}^t_0\varepsilon_{33} = {}^t_0e_{33} + {}^t_0\eta_{33} = {}^t_0z_1/{}^0x_1 + \tfrac{1}{2}\left({}^t_0z_1/{}^0x_1\right)^2 \tag{65b}$$

Note that the load form is a function of the displacement because ${}^t_0x_1 = {}^0x_1 + {}^t_0z_1$.

1. *Material Design Sensitivity Analysis*

The vector of design variables is $\boldsymbol{u}^T = \{A_{10}, A_{20}, A_{30}, k\}$. The variations of the energy and load linear forms with respect to the material design variables can be obtained from Eq. (41), using

$$a_u^*({}^t_0\boldsymbol{z}; {}_0\boldsymbol{z}', {}_0\bar{\boldsymbol{z}}) = \int_{{}^0_\Omega} {}_0D_{ijrs}\, {}_0e'_{ij}\, {}_0\bar{e}_{rs}\, {}^0x_1\, {}^0\mathrm{d}\Omega + \int_{{}^0_\Omega} \left({}^t_0S_{ij}\, {}_0\bar{\eta}'_{ij} + {}^t_0S_{33}\, {}_0\bar{\eta}'_{33} \right) {}^0x_1\, {}^0\mathrm{d}\Omega \tag{66}$$

and

$$a'_{\delta u}({}^t_0\boldsymbol{z}, {}_0\bar{\boldsymbol{z}}) = \int_{{}^0_\Omega} \left[\left({}^t_0S_{ij}\right)' {}^t_0\bar{\varepsilon}_{ij} + \left({}^t_0S_{33}\right)' {}^t_0\bar{\varepsilon}_{33} \right] {}^0x_1\, {}^0\mathrm{d}\Omega \tag{67}$$

where $D_{ijr3} = 0$ for $r \neq 3$, and

$${}_0e'_{ij} = \tfrac{1}{2}\left({}_0z'_{i,j} + {}_0z'_{j,i} + {}^t_0z_{k,i}\, {}_0z'_{k,j} + {}^t_0z_{k,j}\, {}_0z'_{k,i}\right) \tag{68a}$$

$${}_0\bar{e}_{ij} = \tfrac{1}{2}\left({}_0\bar{z}_{i,j} + {}_0\bar{z}_{j,i} + {}^t_0z_{k,i}\, {}_0\bar{z}_{k,j} + {}^t_0z_{k,j}\, {}_0\bar{z}_{k,i}\right) \tag{68b}$$

$${}_0\bar{\eta}'_{ij} = \tfrac{1}{2}\left({}_0z'_{k,i}\, {}_0\bar{z}_{k,j} + {}_0z'_{k,j}\, {}_0\bar{z}_{k,i}\right) \tag{68c}$$

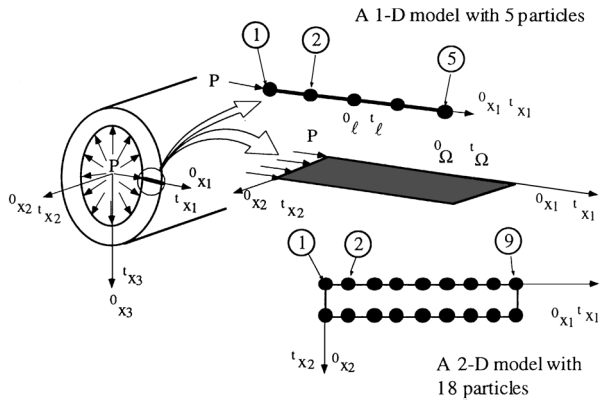

Fig. 5 Infinitely long rubber tube.

for $i, j, k = 1, 2$, and

$$
\begin{aligned}
{}_0e'_{33} &= \left[1 + \left({}^t_0z_1/{}^0x_1\right)\right]\left({}_0z'_1/{}^0x_1\right)\\
{}_0\bar{e}_{33} &= \left[1 + \left({}^t_0z_1/{}^0x_1\right)\right]\left({}_0\bar{z}_1/{}^0x_1\right)\\
{}_0\bar{\eta}'_{33} &= \left({}_0\bar{z}_1/{}^0x_1\right)\left({}_0z'_1/{}^0x_1\right)
\end{aligned}
\tag{68d}
$$

The variation of the load form contains a displacement derivative as

$$
\mathcal{L}_{\delta u}({}_0\bar{z}) = \int_{{}_0\Gamma} P\ {}_0z'_1\ {}_0\bar{z}\ {}^0\mathrm{d}\Gamma \tag{69}
$$

Therefore, the sensitivity equation corresponding to Eq. (41) is

$$
a^*_u\left({}^t_0z;\ {}_0z',\ {}_0\bar{z}\right) - \int_{{}_0\Gamma} P\ {}_0z'_1\ {}_0\bar{z}\ {}^0\mathrm{d}\Gamma = a'_{\delta u}\left({}^t_0z,\ {}_0\bar{z}\right)
\qquad \text{for all} \quad {}_0\bar{z} \in {}_0Z_\tau \tag{70}
$$

The material DSA is implemented using the direct differentiation method. For this example, the material properties are $A_{10} = 0.373$ MPa, $A_{20} = -0.031$ MPa, $A_{30} = 0.005$ MPa, and $k = 2.0 \times 10^4$ MPa. Five particles with support size $a = 15$ mm, four integration zones, and a two-point quadrature are employed for structural analysis and DSA.

The sensitivity results are verified using the forward finite difference with a perturbation $\delta\boldsymbol{u}^T = \{0.0005^*A_{10}, 0, 0, 0\}$. In Table 1, $\psi(\boldsymbol{u} + \delta\boldsymbol{u})$ and $\psi(\boldsymbol{u})$ are displacements at the perturbed and initial designs, respectively; $\delta\psi$ is the finite difference result, i.e., $\psi(\boldsymbol{u} + \delta\boldsymbol{u}) - \psi(\boldsymbol{u})$; ψ' is the predicted displacement variation using sensitivity coefficients, i.e., $\{\partial\psi/\partial\boldsymbol{u}\}^T \cdot \delta\boldsymbol{u}$; and $\psi'/\delta\psi\%$ is the accuracy measurement of sensitivity coefficients. Under the $\psi'/\delta\psi\%$ column, a value closer to 100% indicates that the sensitivity prediction is more accurate.

For the two-dimensional example, 18 particles with a support size of $a = 4.501$ mm in both x_1 and x_2 directions, and 4 integration zones with a 3×3 quadrature rule are employed for structural analysis and DSA. The material properties are $A_{10} = 0.373$ MPa, $A_{20} = -0.031$ MPa, $A_{30} = 0.005$ MPa, and $k = 1.0 \times 10^6$ MPa. The sensitivity results are verified to be accurate, using the forward finite difference with a perturbation $\delta\boldsymbol{u}^T = \{0.001, 0, 0, 0\}$, as shown in Table 2.

2. Shape Design Sensitivity Analysis

For shape DSA, the material derivatives of the energy and load linear forms of the one-dimensional axisymmetric problem can be obtained from Eq. (57), using

$$
\begin{aligned}
a^*_{0_\Omega}\left({}^t_0z;\ {}_0\dot{z},\ {}_0\bar{z}\right) = \int_{{}_0\Omega} &\left({}_0D_{1111}\ {}_0\dot{e}_{11}\ {}_0\bar{e}_{11} + {}_0D_{1133}\ {}_0\dot{e}_{11}\ {}_0\bar{e}_{33}\right.\\
&\left. + {}_0D_{3311}\ {}_0\dot{e}_{33}\ {}_0\bar{e}_{11} + {}_0D_{3333}\ {}_0\dot{e}_{33}\ {}_0\bar{e}_{33}\right){}^0x_1\ {}^0\mathrm{d}\Omega\\
&+ \int_{{}_0\Omega} \left({}^t_0S_{11}\ {}_0\dot{\bar{\eta}}_{11} + {}^t_0S_{33}\ {}_0\dot{\bar{\eta}}_{33}\right){}^0x_1\ {}^0\mathrm{d}\Omega
\end{aligned}
\tag{71}
$$

and

$$
\begin{aligned}
a'_V\left({}^t_0z,\ {}_0\bar{z}\right) = &-\int_0^{0_\ell} \left[{}_0D_{1111}\left(1 + {}^t_0z_{1,1}\right)^2\ {}^t_0z_{1,1}V_1\ {}_0\bar{z}_{1,1}\right.\\
&+ {}_0D_{1133}\left(1 + \frac{{}^t_0z_1}{{}^0x_1}\right)\frac{{}^t_0z_1V_1}{{}^0x_1^2}\left(1 + {}^t_0z_{1,1}\right){}_0\bar{z}_{1,1}\\
&+ {}_0D_{3311}\left(1 + {}^t_0z_{1,1}\right){}_0z_{1,1}V_1\left(1 + \frac{{}^t_0z_1}{{}^0x_1}\right)\frac{{}_0\bar{z}_1}{{}^0x_1}\\
&\left.+ {}_0D_{3333}\left(1 + \frac{{}^t_0z_1}{{}^0x_1}\right)^2\frac{{}^t_0z_1V_1}{{}^0x_1^2}\frac{{}_0\bar{z}_1}{{}^0x_1}\right]{}^0x_1\ {}^0\mathrm{d}x_1\\
&- \int_0^{0_\ell} \left[{}^t_0S_{11}\left(1 + 2\,{}^t_0z_{1,1}\right)V_{1,1}\ {}_0\bar{z}_{1,1}\right.\\
&\left.+ {}^t_0S_{33}\left(1 + 2\frac{{}^t_0z_1}{{}^0x_1}\right)\frac{{}_0\bar{z}_1V_1}{{}^0x_1^2}\right]{}^0x_1\ {}^0\mathrm{d}x_1 + \int_0^{0_\ell} \left[{}^t_0S_{11}\left(1 + {}^t_0z_{1,1}\right){}_0\bar{z}_{1,1}\right.\\
&\left.+ {}^t_0S_{33}\left(1 + \frac{{}^t_0z_1}{{}^0x_1}\right)\frac{{}_0\bar{z}_1}{{}^0x_1}\right]\left(V_1 + {}^0x_1V_{1,1}\right){}^0\mathrm{d}x_1
\end{aligned}
\tag{72}
$$

Note that the material derivative of the load form contains a displacement derivative as

$$
\left[\mathcal{L}_{0_\Omega}({}_0\bar{z})\right]' = P({}_0\dot{z}_1 + V_1)\ {}_0\bar{z}_1 + P^0x_1({}_0\dot{\bar{z}}_1) \tag{73}
$$

Therefore, the sensitivity equation in Eq. (57) becomes

$$
\begin{aligned}
a^*_{0_\Omega}\left({}^t_0z;\ {}_0\dot{z},\ {}_0\bar{z}\right) - P\ {}_0\dot{z}_1\ {}_0\bar{z}_1 &= \mathcal{L}_V({}_0\bar{z}) - a'_V\left({}^t_0z,\ {}_0\bar{z}\right) + \mathcal{L}_{0_\Omega}({}_0\dot{\bar{z}})\\
&\quad - a_{0_\Omega}\left({}^t_0z,\ {}_0\dot{\bar{z}}\right), \qquad \text{for all} \quad {}_0\bar{z} \in {}_0Z
\end{aligned}
\tag{74}
$$

where

$$
\mathcal{L}_V({}_0\bar{z}) = P\ V_1\ {}_0\bar{z}_1 \tag{75}
$$

Table 1 Verification of displacement sensitivity for material property A_{10} for one-dimensional axisymmetric example

Displacement $z1$	$\psi(\boldsymbol{u} + \delta\boldsymbol{u})$	$\psi(\boldsymbol{u})$	$\delta\psi$	ψ'	$\psi'/\delta\psi\%$
Node 1	1.543696E+2	1.543806E+2	−1.1030E−3	−1.1030E−3	100.0
Node 2	1.508222E+2	1.508331E+2	−1.0956E−3	−1.0956E−3	100.0
Node 3	1.473825E+2	1.473934E+2	−1.0878E−3	−1.0878E−3	100.0
Node 4	1.440425E+2	1.440533E+2	−1.0795E−3	−1.0795E−3	100.0
Node 5	1.408056E+2	1.408163E+2	−1.0709E−3	−1.0709E−3	100.0

Table 2 Verification of displacement sensitivity for material property A_{10} of two-dimensional axisymmetric example

Displacement $z1$	$\psi(\boldsymbol{u} + \delta\boldsymbol{u})$	$\psi(\boldsymbol{u})$	$\delta\psi$	ψ'	$\psi'/\delta\psi\%$
Node 1	0.1542833E+2	0.1542240E+2	−0.59269E−2	−0.59235E−2	99.9
Node 2	0.1524966E+2	0.1524375E+2	−0.59072E−2	−0.59038E−2	99.9
Node 3	0.1507366E+2	0.1506777E+2	−0.58869E−2	−0.58836E−2	99.9
Node 4	0.1490028E+2	0.1489442E+2	−0.58661E−2	−0.58627E−2	99.9
Node 5	0.1472953E+2	0.1472369E+2	−0.58447E−2	−0.58414E−2	99.9
Node 6	0.1456135E+2	0.1455553E+2	−0.58228E−2	−0.58195E−2	99.9
Node 7	0.1439573E+2	0.1438993E+2	−0.58003E−2	−0.57970E−2	99.9
Node 8	0.1423262E+2	0.1422684E+2	−0.57774E−2	−0.57741E−2	99.9
Node 9	0.1407201E+2	0.1406625E+2	−0.57540E−2	−0.57507E−2	99.9

Table 3 Verification of displacement sensitivity for shape design variables for one-dimensional axisymmetric example

Displacement $z1$	$\psi(\boldsymbol{u}+\delta\boldsymbol{u})$	$\psi(\boldsymbol{u})$	$\delta\psi$	ψ'	$\psi'/\delta\psi\%$
Node 1	1.547744E+1	1.547701E+1	4.281E−4	4.279E−4	100.0
Node 2	1.512333E+1	1.512289E+1	4.441E−4	4.441E−4	100.0
Node 3	1.477888E+1	1.477842E+1	4.591E−4	4.591E−4	100.0
Node 4	1.444478E+1	1.444431E+1	4.729E−4	4.728E−4	100.0
Node 5	1.411996E+1	1.411948E+1	4.856E−4	4.855E−4	100.0

Table 4 Verification of displacement sensitivity for material property A_{10} of the two-dimensional plane strain example

Displacement	$\psi(\boldsymbol{u}+\delta\boldsymbol{u})$	$\psi(\boldsymbol{u})$	$\delta\psi$	ψ'	$\psi'/\delta\psi\%$
1 $z1$	0.3499085E+1	0.3499084E+1	−0.97179E−6	−0.97357E−3	100.1
1 $z2$	−0.2500702E+0	−0.2500702E+0	0.25450E−8	0.25159E−5	98.9
2 $z1$	0.3499095E+1	0.3499094E+1	−0.96227E−6	−0.96404E−3	100.1
2 $z2$	−0.5001365E+0	−0.5001365E+0	0.66910E−8	0.66372E−5	99.2
7 $z1$	0.2999144E+1	0.2999144E+1	−0.51584E−6	−0.51694E−3	100.2
7 $z2$	−0.2499306E+0	−0.2499304E+0	0.16354E−6	0.16380E−3	100.1
11 $z1$	0.2499563E+1	0.2499563E+1	0.16320E−7	0.16165E−4	99.1
11 $z2$	−0.4997750E+0	−0.4997749E+0	0.12951E−6	0.12979E−3	100.2

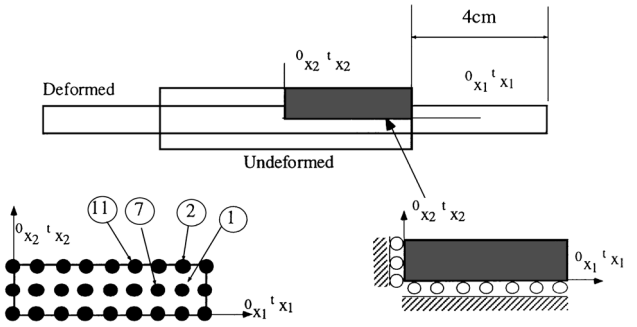

Fig. 6 Two-dimensional rectangular rubber band.

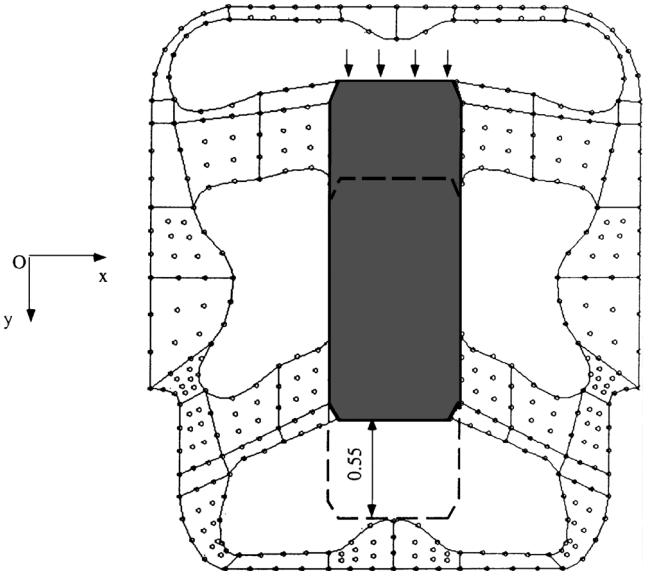

Fig. 7 Particle model of an engine mount.

The shape DSA is implemented using the direct differentiation method. In this example, five particles with support size $a = 10$ mm, four integration zones, and a one-point quadrature are employed for structural analysis and DSA. The inner radius of the tube is defined as the shape design variable. A linear design velocity field is defined for this shape design variable, i.e., $V_1(x_1) = (r_{\text{ext}} - x_1)/(r_{\text{ext}} - r_{\text{int}})$. The sensitivity results of the one-dimensional example are verified to be accurate using the forward finite difference with a perturbation of 0.001 mm, as shown in Table 3.

B. Two-Dimensional Rectangular Rubber Band

A rectangular rubber band with a prespecified displacement is modeled as a two-dimensional plane strain problem, as shown in Fig. 6. The size of the band is $4 \times 1\,\text{cm}^2$. Because of symmetry, only one quarter is analyzed. The material properties are $A_{10} = 0.373$ MPa $A_{20} = -0.031$ MPa, $A_{30} = 0.005$ MPa, and $k = 1.0 \times 10^5$ MPa. The displacements in the x_1 direction are imposed to be 4 cm, as shown in Fig. 6. The energy form of the two-dimensional plane strain problem with the material and shape design sensitivity expressions can be obtained from Secs. IV and V. The variation of the load form vanishes because the external load does not depend on design variables.

For this plane strain example, 27 particles with support size $a = 1.0$ cm in both x_1 and x_2 directions, 4 integration zones, and a 3×3 quadrature rule are used to perform structural analysis and DSA. The material design sensitivity is computed using the direct differentiation method. The sensitivity results are verified to be accurate, using the forward finite differences with a perturbation $\delta\boldsymbol{u}^T = \{0.001, 0, 0, 0\}$, as shown in Table 4.

C. Engine Mount

An engine mount with imposed displacement boundary conditions is modeled as a two-dimensional problem, as shown in Fig. 7. A geometric model is created using MSC/PATRAN.[28] Because of symmetry, only half of the structure is analyzed. Half of the model contains 188 particles and 133 integration zones. Yeoh's strain energy density is employed to describe the hyperelastic material as in Eq. (2). The exterior boundary is assumed to be fixed. The interior metal block (the shaded region in Fig. 7) is treated as a rigid body and the stiffness of the engine mount is viewed as a performance measure. The stiffness is computed using the ratio of the reaction force developed at the final load step and the imposed displacement. The hydrostatic pressures at critical points are also selected as the performance measures.

The analysis is carried out in 25 load steps, due to high nonlinearity of the model and large deformation. Figure 8 shows the fringe plot of the hydrostatic pressure on the deformed engine mount. The hydrostatic pressure is computed from

$$p = k\left({}^t_0 J - 1\right) \tag{76}$$

where k is the bulk modulus and ${}^t_0 J$ is the determinant of the deformation gradient.

Eight shape design parameters, the x and y coordinates of four control points (grid points 8, 12, 29, and 33) on the boundary as shown in Fig. 9, are selected for this problem. Eight corresponding

Table 5 Verification of stiffness and pressure sensitivity for engine mount

Performance measure	Design parameter no.	$\psi(\boldsymbol{u})$	$\psi(\boldsymbol{u}+\delta\boldsymbol{u})$	$\delta\psi$	$\dot{\psi}$	$\dot{\psi}\times\delta u/\delta\psi\%$
Stiffness	1	1.8963177	1.8912487	−0.5069D−02	−0.5117D+01	100.9
	2	1.8963177	1.8955871	−0.73062D−03	−0.72934D+00	99.8
	3	1.8963177	1.8959556	−0.36215D−03	−0.37556D+00	103.7
	4	1.8963177	1.8967045	0.38677D−03	0.38895D+00	100.6
Pressure no. 40	1	−346.9361	−346.9215	0.14616D−01	0.14380D+02	98.4
No. 48	1	326.2706	326.2583	−0.12300D−01	−0.12107D+02	98.4
No. 50	1	201.8209	201.8162	−0.47118D−02	−0.46218D+01	98.1
No. 55	1	475.8586	475.8148	−0.43801D−01	−0.43047D+02	98.3
No. 118	1	−244.8332	−247.4717	−0.26385D+01	−0.26735D+04	101.3
No. 40	2	−346.9361	−346.9251	0.11050D−01	0.11136D+02	100.8
No. 48	2	326.2706	326.2615	−0.91679D−02	−0.92386D+01	100.8
No. 50	2	201.8209	201.8172	−0.37362D−02	−0.37663D+01	100.8
No. 55	2	475.8586	475.8247	−0.33876D−01	−0.34146D+02	100.8
No. 118	2	−244.8332	−243.5505	0.12827D+01	0.12881D+04	100.4
No. 40	3	−346.9361	−346.9456	−0.95075D−02	−0.95165D+01	100.1
No. 48	3	326.2706	326.2783	0.76456D−02	0.76566D+01	100.1
No. 50	3	201.8209	201.8244	0.34570D−02	0.34572D+01	100.0
No. 55	3	475.8586	475.8889	0.30361D−01	0.30372D+02	100.0
No. 118	3	−244.8332	−246.4168	−0.15836D+01	−0.15837D+04	100.0
No. 40	4	−346.9361	−346.9396	−0.34887D−02	−0.35025D+01	100.4
No. 48	4	326.2706	326.2735	0.28423D−02	0.28537D+01	100.4
No. 50	4	201.8209	201.8222	0.12526D−02	0.12580D+01	100.4
No. 55	4	475.8586	475.8696	0.11011D−01	0.11056D+02	100.4
No. 118	4	−244.8332	−245.5486	−0.71542D+00	−0.71932D+03	100.5

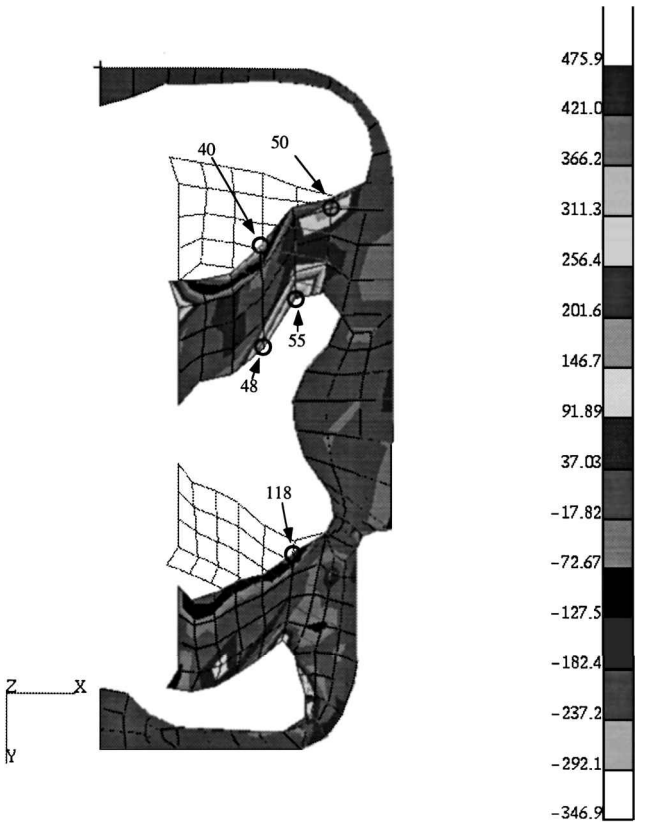

Fig. 8 Pressure fringe plot on deformed structure.

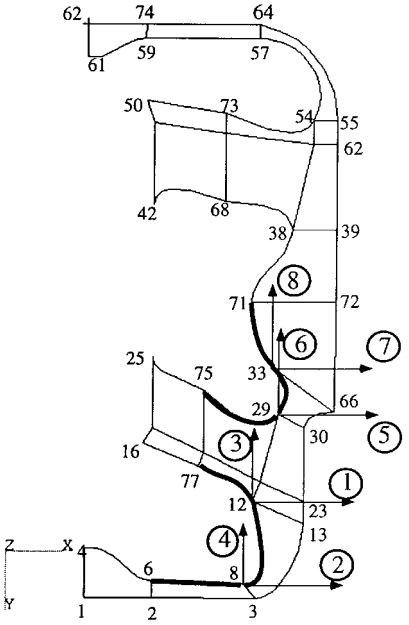

Fig. 9 Design parametrization.

design velocity fields are computed using the boundary displacement method of the design sensitivity analysis and optimization tool.[29] Equation (57) is used to compute the design sensitivity of the displacement for each shape design parameter. The design sensitivities of the hydrostatic pressure at selected critical points and the stiffness of the structure are computed using Eq. (59). The results are verified using the forward finite difference with perturbations of 0.001 for each design parameter as shown in Table 5.

VIII. Conclusions

A continuum-based DSA method for hyperelastic structures using RKPM was presented. Both the material and shape DSA methods for hyperelastic structures were developed. The proposed DSA methods were demonstrated to be quite accurate using various one- and two-dimensional examples. Shape DSA and optimization using the meshless method hold a great potential to remedy mesh distortion problems that occur using traditional finite element methods. Currently, a shape optimization capability using the RKPM is being developed to explore and to demonstrate the true advantages of applying RKPM to support shape design optimization.

Acknowledgment

This research was supported by the Army Automotive Research Center of Excellence for Modeling and Simulation.

References

[1]Monaghan, J. J., "An Introduction to SPH," *Computer Physics Communications*, Vol. 48, No. 1, 1988, pp. 89–96.

[2]Nayroles, B., Touzot, G., and Villon, P., "Generalizing the Finite Element Method: Diffuse Approximation and Diffuse Elements," *Computational Mechanics*, Vol. 10, No. 5, 1992, pp. 307–318.

[3]Belytschko, T., Lu, Y. Y., and Gu, L., "Element-Free Galerkin Methods," *International Journal for Numerical Methods in Engineering*, Vol. 37, No. 2, 1994, pp. 229–256.

[4]Lu, Y. Y., Belytschko, T., and Gu, L., "A New Implementation of the Element Free Galerkin Method," *Computer Methods in Applied Mechanics and Engineering*, Vol. 113, Nos. 3, 4, 1994, pp. 397–414.

[5]Liu, W. K., Jun, S., and Zhang, Y. F., "Reproducing Kernel Particle Methods," *International Journal for Numerical Methods in Engineering*, Vol. 20, No. 10, 1995, pp. 1655–1679.

[6]Liu, W. K., Jun, S., Sihling, D. T., Chen, Y., and Hao, W., "Multiresolution Reproducing Particle Method for Computational Fluid Dynamics," *International Journal for Numerical Methods in Fluids*, Vol. 24, No. 12, 1997, pp. 1391–1415.

[7]Chen, J. S., Pan, C., and Wu, T. C., "Large Deformation Analysis of Rubber Based on a Reproducing Kernel Particle Method," *Computational Mechanics*, Vol. 19, No. 3, 1997, pp. 153–168.

[8]Chen, J. S., Pan, C., Wu, T. C., and Liu, W. K., "Reproducing Kernel Particle Methods for Large Deformation Analysis of Nonlinear Structures," *Computer Methods in Applied Mechanics and Engineering*, Vol. 139, Nos. 1–4, 1996, pp. 195–227.

[9]Liu, W. K., Li, S., and Belytschko, T., "Moving Least Square Reproducing Kernel Method (I) Methodology and Convergence," *Computer Methods in Applied Mechanics and Engineering*, Vol. 143, Nos. 1, 2, 1997, pp. 113–154.

[10]Choi, K. K., and Santos, J. L. T., "Design Sensitivity Analysis of Non-Linear Structural Systems Part I: Theory," *International Journal for Numerical Methods in Engineering*, Vol. 24, No. 11, 1987, pp. 2039–2055.

[11]Santos, J. L. T., and Choi, K. K., "Sizing Design Sensitivity Analysis of Nonlinear Structural Systems with Existing Finite Element Code," *ANSYS Conference Proceedings*, 1987, pp. 1.35–1.56.

[12]Choi, K. K., and Santos, J. L. T., "Design Sensitivity Analysis of Non-Linear Structural Systems Part II: Numerical Method," *International Journal for Numerical Methods in Engineering*, Vol. 26, No. 9, 1988, pp. 2097–2114.

[13]Park, J. S., and Choi, K. K., "Design Sensitivity Analysis of Critical Load Factor for Nonlinear Structural Systems," *Computers and Structures*, Vol. 36, No. 5, 1990, pp. 823–838.

[14]Choi, K. K., "Design Sensitivity Analysis of Nonlinear Structures II," *Structural Optimization: Status & Promise*, edited by M. P. Kamat, Progress in Astronautics and Aeronautics, AIAA, Washington, DC, 1993, Chap. 16, pp. 407–446.

[15]Santos, J. L. T., and Choi, K. K., "Shape Design Sensitivity Analysis of Nonlinear Structural Systems," *Structural Optimization*, Vol. 4, No. 1, 1992, pp. 23–35.

[16]Choi, K. K., and Duan, W., "Shape Design Sensitivity Analysis of Hyperelastic Solids," *The First World Congress of Structural and Multidisciplinary Optimization*, edited by N. Olhoff and G. I. N. Rozvany, Elsevier Science, Tarrytown, NY, 1996, pp. 421–428.

[17]Choi, K. K., and Duan, W., "Design Sensitivity Analysis Shape Design Optimization of Structural Components with Hyperelastic Material," *Computer Methods in Applied Mechanics and Engineering* (submitted for publication).

[18]Haug, E. J., Choi, K. K., and Komkov, V., *Design Sensitivity Analysis of Structural Systems*, Academic, New York, 1985, Chap. 3.

[19]Arora, J. S., and Cardoso, J. B., "Variational Principles for Shape Design Sensitivity Analysis," *AIAA Journal*, Vol. 30, No. 2, 1992, pp. 538–547.

[20]Tortorelli, D. A., "Sensitivity Analysis for Nonlinear Constrained Elastostatic Systems," *International Journal for Numerical Methods in Engineering*, Vol. 33, No. 8, 1992, pp. 1643–1660.

[21]"ABAQUS, ABAQUS User's Manual," Hibbit, Karlsson and Sorensen, Inc., 100 Midway Street, Providence, RI 02906-4402, 1990.

[22]Bathe, K. J., *Finite Element Procedures*, Prentice–Hall, Englewood Cliffs, NJ, 1996, Chap. 6.

[23]Yeoh, O. H., "Characterization of Elastic Properties of Carbon Black Filled Rubber Vulcanizates," *Rubber Chemistry and Technology*, Vol. 63, 1990, pp. 792–805.

[24]Penn, R. W., "Volume Changes Accompanying the Extension of Rubber," *Transactions of the Society of Rheology*, Vol. 14, No. 4, 1970, pp. 509–517.

[25]Chen, J. S., Wu, T. C., and Pan, C., "A Pressure Projection Method for Nearly Incompressible Rubber Hyperelasticity, Part I: Theory," *Journal of Applied Mechanics*, Vol. 63, No. 4, 1996, pp. 862–868.

[26]Chen, J. S., Wu, T. C., and Pan, C., "A Pressure Projection Method for Nearly Incompressible Rubber Hyperelasticity, Part II: Applications," *Journal of Applied Mechanics*, Vol. 63, No. 4, 1996, pp. 869–876.

[27]Choi, K. K., and Chang, K. H., "A Study of Design Velocity Field Computation for Shape Optimal Design," *Finite Elements in Analysis and Design*, Vol. 15, No. 4, 1994, pp. 317–341.

[28]"MSC/PATRAN, MSC/PATRAN User Manual," MacNeal-Schwendler Corp., Los Angeles, CA, 1996.

[29]Chang, K. H., Choi, K. K., Tsai, C. S., Chen, C. J., Choi, B. S., and Yu, X., "Design Sensitivity Analysis and Optimization Tool (DSO) for Shape Design Applications," *Computing Systems in Engineering*, Vol. 6, No. 2, 1995, pp. 151–175.

A. D. Belegundu
Associate Editor